



ACADEMIC
PRESS

Available online at www.sciencedirect.com

SCIENCE  DIRECT[®]

Journal of Colloid and Interface Science 263 (2003) 133–143

JOURNAL OF
**Colloid and
Interface Science**

www.elsevier.com/locate/jcis

Electrokinetic mixing vortices due to electrolyte depletion at microchannel junctions

Paul Takhistov, Ksenia Duginova, and Hsueh-Chia Chang *

Department of Chemical Engineering, University of Notre Dame, Notre Dame, IN 46556, USA

Received 15 July 2002; accepted 12 March 2003

Abstract

Due to electric field leakage across sharp corners, the irrotational character of Ohmic electroosmotic flow is violated. Instead, we demonstrate experimentally and theoretically evidence of electrolyte depletion and vortex separation in electroosmotic flow around a junction between wide and narrow channels. When the penetration length of the electric field exceeds the width of the narrow channel and if the electric field is directed from the narrow to the wide channel, the electromigration of ions diminishes significantly at the junction end of the narrow channel due to this leakage. Concentration depletion then develops at that location to maintain current balance but it also increases the corner zeta potential and the local electroosmotic slip velocity. A back pressure gradient hence appears to maintain flow balance and, at a sufficient magnitude, generates a pair of vortices.

© 2003 Elsevier Science (USA). All rights reserved.

Keywords: Microfluidics; Electrokinetic flow; Electroosmosis; Zeta potential; Polarization; Vorticity

1. Introduction

Microfluidics, the study of fluid transport in micrometer-scale devices, is a rapidly emerging field with a broad range of applications [1]. Areas of utility include the development of biochips for high-throughput drug screening, biosensors for medical and environmental diagnostics, quality control for industrial processes such as food preparation, and detection of chemical warfare agents for the military. Physical characterization of micrometer-scale transport phenomena is in its formative stages and is consequently of great interest to biochemists, physicists, and engineers. Current research goals for advanced microfluidic systems include multiple processes per test, multiple tests per use, and multiple uses per chip. A crucial direction focuses on efficient transfer of colloidal suspensions [2] through microchannels of varying size and geometry. Such colloids can carry a large variety of antigens or drug compounds in microscopic quantities.

Due to its high maneuverability, electrokinetic flow has become the microfluidic transport mechanism of choice over pressure-driven and centrifugally driven flows. Electrodes can be placed at arbitrary locations within a network of

microchannels on a multitasking chip. By activating the proper electrodes via underlying microcircuitry, the samples can be transported by the resulting electric fields to different stations in the network. The electrodes that are used to drive electroosmotic flow of the electrolyte solution and the samples can also be used as sensors/detectors [3]. Colloidal transport, an active microfluidic research area, can be achieved by driving the colloids electrophoretically with the electric fields. Even nonelectrolyte liquid samples can be transported electrokinetically with proper designs [4].

A major hydrodynamic advantage over pressure-driven flow is the flat velocity profile of electroosmotic flow [5] for fully developed flow in a channel whose width is much larger than the Debye layer thickness (<100 nm). This flat velocity results because the electrostatic body force exists only within the thin Debye layer with charge separation and hence is effectively a tangential surface force captured by the Smoluchowski slip velocity. This produces a much smaller hydrodynamic resistance for the flat electroosmotic flow than the nonuniform velocity profiles of body-force (pressure or centrifugal forces)-driven flow. Specifically, the average velocity of electroosmotic flow is independent of the thinnest transverse dimension d of the microchannel, whereas that for pressure-driven flow scales as d^2 at the same driving force [6]. This scaling imposes a lower limit

* Corresponding author.

E-mail address: hsueh-chia.chang.2@nd.edu (H.-C. Chang).

on the dimension of microdevices that can utilize pressure-driven flow.

However, there are numerous design issues that must be overcome before electrokinetic flow can become a common means of transport in future generations of biochips. Proteins tend to denature in high electric fields. Proteins precipitate and colloids aggregate at corners, particularly at junctions, as we shall demonstrate. Although the flat electroosmotic velocity profile reduces Taylor dispersion, hydrodynamic dispersion remains a problem around turns and at junctions [7]. This is particularly acute when pressure-driven back flow produces a nonuniform velocity profile [8] or even vortices [9] in electroosmotic flow when the zeta potential is not uniform. There is even concern that fingering can occur at the back of an electrolyte sample due to the lower electric field and the lower zeta potential in the presence of the sample. This, however, has proved to be insignificant for most biochips [10].

Due to the small diffusivity of long proteins and colloids, diffusive contacts of these entities are often excessively long in diagnostic kits and high-throughput drug screening. Miniature mixing chambers are thus required in the microchannel networks. Because hydrodynamic dispersion is weak for flat electroosmotic flows, reactant mixing becomes problematic. Severely curved channels that utilize Taylor dispersion for reagent mixing would consume excessive channel lengths. What would be more desirable is microvortices that can be generated within the microchannels. Such vortices can also be used to break up protein precipitates or colloid aggregates. Mechanical stirrers, oscillating bubble mixers, and piezoelectric devices have been suggested as possible mixing elements. However, mechanical mixers are quite unreliable for nondisposable microfluidic chips. Moreover, it has been known for a long time that, without a pressure gradient and with uniform zeta potential, the viscous electrokinetic streamlines within dielectric channels are identical to the electric field lines [5,11]. Since the latter are the gradient of the electric potential, the velocity field is irrotational and cannot sustain vortices. It is hence extremely difficult to generate vortices in electrokinetic flow unless one introduces nonuniform zeta potential and/or pressure body force.

In this paper, we report and analyze two new phenomena in electroosmotic flow of electrolytes and electrophoretic flow of colloids in microchannels. Both occur at the junction of a narrow channel with a wide channel. A large aspect ratio and an acute corner angle are shown to produce significant ion depletion at the inner junction corner. The accompanying local zeta potential change is then shown to produce vortices in the electroosmotic flow within the narrow channel and corner aggregation of colloids. The large aspect ratio produces a large change in the tangential electric field and the corner allows significant field leakage through the dielectric channel material. Both conspire to produce these two new phenomena. We numerically determine the critical

applied fields for both phenomena to occur for a particular junction geometry.

2. Electrostatic–hydrodynamic fundamentals and similitude for insulating walls

Microdevices fabricated from photo- or chemical etching technologies are typically planar chips. Their microchannels hence have a normal dimension d (gap separation across the chip) that is usually small compared to the other transverse length scales and is definitely smaller than the usual channel length. Thus, one can depth-average the hydrodynamics and electrostatics to produce planar governing equations. This depth-averaging is particularly simple for electroosmotic flow due to its flat velocity profiles in this thin direction. This flat velocity profile can be distorted in the other transverse direction across the channel due to back pressure. However, the profile across the thin direction remains flat. For ionic strengths of realistic electrolytes larger than 10^{-10} M, the Debye thickness does not exceed several hundred nano-meters. Hence, provided the gap separation d is more than 10 μm , which is true for all microchannels, the velocity profile in the normal direction is flat and any variation in the same direction can be neglected. Depth averaging is hence valid and simple for fluid flow in electrokinetic microdevices. Assuming insulating conditions on the two planes of the chip, which is usually valid if the surrounding fluid is air, the electric potential φ is also independent of the thin direction. The same can be said about the steady concentration fields, as there is obviously no solute flux across the planes. As a result, all the governing equations are simple two-dimensional analogs of their original versions,

$$\nabla \cdot (\varepsilon \nabla \varphi) = -\rho, \quad (1)$$

$$\nabla^4 \psi = 0, \quad (2)$$

$$j_{\pm} = -D_{\pm} \nabla C_{\pm} - \frac{F z_{\pm} D_{\pm} C_{\pm}}{RT} \nabla \varphi + C_{\pm} u, \quad (3)$$

where ∇ is the gradient operator, ε is the dielectric permittivity, which is different for the solid and the electrolyte, $\rho = F \sum_{i=1}^2 z_i C_i$ is the electric charge density for our idealized binary electrolyte with molar concentrations C_{\pm} ,

$$u = \begin{pmatrix} \partial \psi / \partial y \\ -\partial \psi / \partial x \end{pmatrix}$$

is the planar velocity field expressed in terms of the stream function ψ , F is the Faraday constant, D_{\pm} are the ion diffusivities, and z_{\pm} are the ionic valences. The contributions of diffusion, electromigration, and convection are evident in the steady molar flux j_{\pm} in (3) for each ion. Note that we have retained the full viscous flow biharmonic equation, instead of the usual potential flow equation, to allow for the possibility of pressure-gradient back flow and vortices. The usual potential flow formulation is irrotational and rules out both a priori.

Due to the strong electrostatic attraction between the oppositely charged ions, electroneutrality ($\rho = 0$) is obeyed everywhere except near the dielectric wall boundary with the fluid. Within the thin (<100 nm) Debye layer there, charge separation can occur to screen the natural surface charge on the dielectric wall. The potential drop across this charged layer is the zeta potential ζ and the electroosmotic slip velocity in the bulk is determined by ζ and the tangential field [5], as we shall specify later. In the electrostatic problem, however, we shall neglect the potential drop across the double layer and assume that the potential drops across both the Helmholtz and diffusive parts of the double layer do not affect the electric field and the leakage. In essence, we assume that the electrolyte ions screen and cancel the surface charges in the thin Debye layer and both charges are unaffected by the current—the Debye capacitor is not charged by the current. Thus, the potential away from the Debye layer, which is specified by the current, is unaffected by the Debye layer.

Hence, equating the ion concentrations for this electroneutral condition,

$$C^+ = C^- = C, \quad (4)$$

the electrostatic Poisson problem (1) becomes the Laplace equation with nonconstant coefficients,

$$\nabla \cdot (\varepsilon \nabla \varphi) = 0. \quad (5)$$

Multiplying each of the two ion-flux equations by Fz_i and subtracting to obtain the current density J , we find that the convection contributions cancel for symmetric ions ($|z_+| = |z_-| = z$) under electroneutral conditions,

$$\begin{aligned} J &= zF(j_+ - j_-) \\ &= -Fz(D_+ - D_-)\nabla C - \frac{F^2z^2}{RT}C(D_+ + D_-)\nabla\varphi. \end{aligned} \quad (6)$$

Solute flux balance then stipulates

$$\nabla \cdot J = 0 \quad (7)$$

within the fluid phase or, invoking the Gauss Divergence Theorem,

$$\oint_{\Gamma} J \cdot n \, ds = 0, \quad (8)$$

where Γ is a closed contour in the fluid phase. The total current I carried by the ions must be constant across any curve Λ that connects the two walls of a channel. To show this, we define Γ by two wall boundaries Σ and two curves Λ across the microchannel. Since there cannot be any solute flux into the wall,

$$J \cdot n|_{\Sigma} = 0 \quad (9)$$

and (8) stipulates that the total current,

$$I = \int_{\Lambda} J \cdot n \, ds, \quad (10)$$

is constant for every curve Λ that connects the two opposing walls of a microchannel. There must be a net current balance within the channel and this current is supplied by only electromigration if the concentration field is uniform. The usual Ohmic relationship between current and voltage applies in this limit of uniform concentration and hence constant electric field in a straight channel. We shall show that, if the concentration is not uniform in a straight channel, the contribution of diffusive flux to the current will stipulate a nonconstant electric field along the channel.

The dielectric solids (acrylic, glass, PDMS, etc.) used to construct microchips typically have low relative dielectric permittivities $\varepsilon_r = \varepsilon/\varepsilon_0$ between 3 and 4, while the relative permittivity of distilled water is 81. Hence, to a leading order, the solid can be assumed to be an insulator with no field leakage. Thus, if the jump in the potential gradient across the double layer is omitted, the normal derivative of φ at Σ vanishes and (9) stipulates that φ and C obey the same Neumann conditions at the liquid–solid interface Σ ,

$$\frac{\partial \varphi}{\partial n} \Big|_{\Sigma} = \frac{\partial C}{\partial n} \Big|_{\Sigma} = 0, \quad (11)$$

and the Laplace equation (5) needs only be solved in the fluid phase,

$$\nabla^2 \varphi = 0, \quad (12)$$

which also stipulates

$$\oint_{\Gamma} \nabla \varphi \cdot n \, ds = 0 \quad (13)$$

over any closed curve Γ in the fluid phase.

Comparing (7) to (12) and (8) to (13) and noting (11), it is evident that, in the case of an insulating wall, a particular solution to the electrostatic and mass transport problem contains a uniform concentration field $C = C_{\infty}$ that is independent of position. For this solution, the solute flux balance (7) collapses into the Laplace equation (10) and the current flux density is due entirely to electromigration,

$$J_{\text{Ohm}} = -\sigma \nabla \varphi, \quad (14)$$

where $\sigma = F^2z^2/(RT)C_{\infty}(D_+ + D_-)$ is the conductivity. Moreover, by using two equipotential lines as Λ in (10), the total current

$$I_{\text{Ohm}} = -\sigma \int_{\Lambda} \frac{\partial \varphi}{\partial n} \, ds \quad (15)$$

is constant over any curve Λ . This expression is identical to the usual Ohm's law for a constant electric field, $E_0 = -\partial \varphi / \partial n = \Delta V/l$, where l is the length of the channel over which the voltage drop ΔV occurs.

For this Ohmic solution with an insulating wall, the concentration field is known and uniform and only the Laplace equation (12) needs to be solved for the electric potential φ

with Neumann conditions (11). One can then solve the biharmonic equation (2) for the stream function with the Smoluchowski slip condition for the tangential velocity u_t ,

$$u_t = \frac{\partial \psi}{\partial n} \Big|_{\Sigma} = \frac{\varepsilon \zeta (C)}{\mu} \left(\frac{\partial \varphi}{\partial t} \right)_{\Sigma} = -\frac{\varepsilon \zeta E_t}{\mu} \Big|_{\Sigma}, \quad (16)$$

where $E_t = -\partial \varphi / \partial t$ is the tangential electric field, and the zero normal flux condition (for the fluid)

$$\frac{\partial \psi}{\partial t} \Big|_{\Sigma} = 0. \quad (17)$$

For the acrylic chips used in our experiments, the ζ potential is negative and its absolute value is typically a decreasing function [4,5] of the electrolyte concentration C . In the uniform concentration limit $C = C_{\infty}$, it is a constant independent of position.

For insulating walls, (11) stipulates that the boundary is a field line, whereas the boundary is always a streamline, as seen in (17). Moreover, since the solution of the Laplace equation is always a solution of the biharmonic equation (2), the fact that the electrostatic boundary condition is identical to that of the flow equation means that the field lines and streamlines are identical everywhere. Moreover, the electric potential is also the velocity potential for this purely electroosmotic flow in an insulated channel. The pressure field is also uniform, so that there is no pressure-driven flow.

This is the similitude between electrostatic field lines and electroosmotic streamlines that was first suggested by Overbeek [11] for insulating walls. Cummings et al. [14] have recently shown that the similitude still holds for a perfectly conducting wall with constant potential, viz., without the shielding effects of double layers. However, even without the double layers, finite wall permittivity that is neither zero (insulating) nor infinite (conducting) would render different the boundary conditions for flow and field and hence destroy the similitude. The electric field can penetrate the wall but not the fluid. In fact, as we shall show subsequently, even the familiar Ohm's law (15) is strictly valid only for insulating walls. In this limit, the concentration field is uniform in the fluid. Most importantly, since $E = -\nabla \varphi$ is irrotational, $\nabla \times E = 0$, the resulting planar velocity field is also irrotational and cannot contain any closed vortices. To obtain vortices, one must revoke the Ohmic conditions and, theoretically, the biharmonic Stokes equation (2) must be used instead of the Laplace equation for potential flow. We do so here by introducing finite solid dielectric permittivity and, with it, a nonuniform concentration field, a nonuniform zeta potential, and a pressure field to drive the vortices. We also use the current flux balance (15) and an additional flow balance to estimate the existence condition, location, and strength of the vortices.

3. Vortex formation due to field leakage across corners

Due to the large difference in the solid and liquid permittivities, the insulating wall approximation (11) is a good

one except near sharp channel junctions or corners. Here, a large potential gradient exists across the solid and nonnegligible field leakage exists even with low solid permittivity. This field leakage breaks the similarity between streamlines and electric field lines, as the latter now penetrate the wall and the boundary conditions for electric and velocity fields are different. This immediately implies that the stream function ψ is not a conjugate harmonic pair of φ and it is not a harmonic function that satisfies the Laplace equation. As a result, the streamlines are not the electric field lines, as their boundary conditions now differ, and are no longer irrotational.

In fact, for an ideally sharp corner (a wedge), the tangential field is singular at the corner for a perfectly insulated wall. With finite but small wall permittivity, the fields are no longer singular, but now a large normal field is present at the wedge due to field leakage across the corner. This normal field charges the double layer on the upstream side of the wedge and discharges the one on the downstream side. The leakage also causes a reduction in the tangential electric field on the upstream side of the electric field. The variation in the overpotential and the tangential field around the wedge then produces a converging Smoluchowski slip velocity (16), which also drives a vortex that straddles the inside corner. Its circulation direction is identical to that of the original Ohmic flow around the corner. We examined this microvortex generation mechanism near a semi-infinite wedge in a separate paper [12]. It can only occur for very sharp wedges and very large normal fields.

Here, we scrutinize a different situation with the specific junction geometry shown in Fig. 1, where a narrow channel meets a wide one. The anode is placed at the end of the narrow channel and the cathode at the end of the wide one. As a result, the electric field and current flow from the narrow channel into the wide one. With the negative ζ potential of the acrylic surface, the electroosmotic flow is also in the same direction, toward the cathode. Due to the finite width of

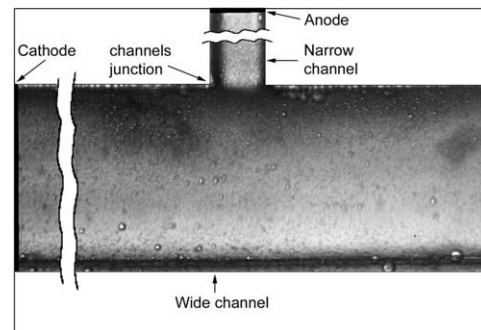


Fig. 1. The actual perpendicular junction of our acrylic chip ($\zeta = -20$ to -50 mV and relative permittivity $\varepsilon = 4$). The wide channel is $400 \mu\text{m}$ wide and 5 cm long, whereas the narrow channel is $80 \mu\text{m}$ wide and 2.5 cm long. They are both about $200 \mu\text{m}$ deep. The anode is placed at the end of the narrow channel and the cathode at the end of the wide channel. Electroosmotic flow and current are toward the cathode in the wide channel, whereas the electrophoretic motion of the latex colloids (negative ζ potential) is toward the anode in the narrow channel.

the narrow channel, its ion flux that carries the currents can be significantly affected by a slight field leakage when the field penetration depth is comparable to the channel width. This current imbalance will be shown to produce vortices different from that near a wedge [12]—they span the entire narrow channel. Hence, with narrow channels, the corners need not be as sharp as the wedges in the mechanism of [12] or the field leakage as severe to produce vortices.

When the leakage is sufficiently severe such that a properly defined penetration length exceeds the width of the narrow channel, the reduction in the electric field spans the entire junction end of the channel. As such, the Ohmic current out of the narrow channel due to electromigration is severely reduced. Unlike the electric field, the current carrying ion flux cannot penetrate the wall and is hence diminished with a weaker electric field. However, far upstream away from the junction, the electric field is unaffected by the leakage. As a result, the Ohmic flux (15) is no longer equal across two Λ curves, one at the junction end and one at the far upstream end of the narrow channel. The same is true for the much wider channel but the current flux imbalance is much less severe.

To increase the total current at the junction end of the narrow channel, the Ohmic condition where current is driven only by electromigration must be violated. Instead, a concentration gradient must be introduced to allow diffusive flux to augment electromigration, as at the original flux density (6).

Since the proton diffusivity is usually higher than that of the anion, $D_+ > D_-$ for most electrolytes whose dominant cations are H^+ ions. Consequently, (6) indicates that, to increase the current out of the narrow channel, the concentration C must have a negative gradient in the electric field direction; viz., the concentration in the narrow channel decreases toward the junction. Around the corner in the wide channel, the effect of field leakage is much less severe and the concentration must return to the original value. Hence, a depletion of electrolyte exists in a length of the narrow channel near the junction, which is equal to the field penetration length and is larger than the channel width.

Note that if the electrodes are reversed, the narrow side of the junction still suffers a weaker field due to leakage. However, an increase in H^+ concentration must occur at its junction end to drive the current into the narrow channel. Whether an electrolyte depletion or buildup occurs hence depends on the electrode configuration!

This electrolyte depletion or buildup can only occur if the field penetration length exceeds the channel width—if the tangential electric field is reduced across the entire narrow channel at the junction. The concentration change in C , in turn, would now cause an opposite change in the wall zeta potential ζ in (16). As a result, an elevated ζ potential exists at the junction end of the narrow channel if depletion occurs in the electrode configuration of Fig. 1. With polarity reversal, a lower ζ potential exists at the same region with electrolyte build up. To obey total flow balance, a positive

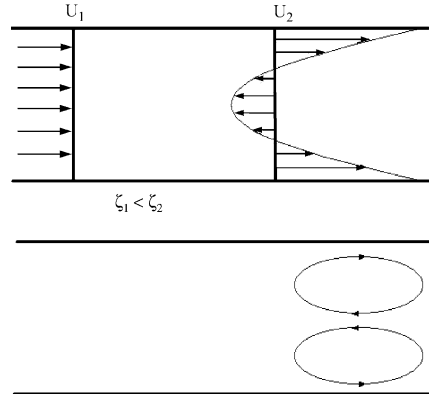


Fig. 2. The flat purely electroosmotic velocity profile at low ζ potential evolves into a mixed pressure-driven/electroosmotic profile in the high- ζ -potential region 2. The slip velocity U_2 is larger than U_1 but the flow rates are identical due to pressure-driven back flow in region 2. A vortex pair symmetric about the center axis appears when the center velocity in region 2 becomes negative.

streamwise pressure gradient must be established to reduce the flow in the high ζ potential region, as shown in Fig. 2. Unlike the flat velocity profile of a pure electroosmotic flow, this mixed pressure-driven and electroosmotic velocity profile has two symmetric maxima across the center line and a minimum at the center line. The velocity at the center line can even be opposite in direction to the average velocity (flow), resulting in two symmetric vortices across the center line in the high- ζ region [9].

Using the unidirectional flow approximation of Fig. 2, the velocity in region 2 with elevated ζ potential can be readily solved for the biharmonic equation (2) with slip condition (16),

$$u_2(y) = \frac{1}{\mu} \frac{\partial p}{\partial x} \left(\frac{y^2}{2} - \frac{d^2}{2} \right) + U_2, \quad (18)$$

where d is half of the channel width and U_2 the slip velocity. Integrating to get the flow rate

$$Q_2 = -\frac{2d^3}{3\mu} \frac{\partial p}{\partial x} + 2dU_2$$

and equating the flow rate of the purely electroosmotic region 1 with a flat velocity profile to $Q_1 = 2dU_1$, one obtains the back-pressure gradient in region 2,

$$\left(\frac{\partial p}{\partial x} \right) = \frac{3\mu}{d^2} (U_2 - U_1). \quad (19)$$

Substituting this into the mixed velocity profile (18) and evaluating the velocity at the center line, we conclude that $u_2(0)$ becomes negative when

$$\frac{U_2}{U_1} = 3. \quad (20)$$

If the electric fields in regions 1 and 2 are roughly the same, the ζ potential ratio would need to exceed

$$\frac{\zeta_2}{\zeta_1} = 3 \quad (21)$$

for vortices to form in region 2.

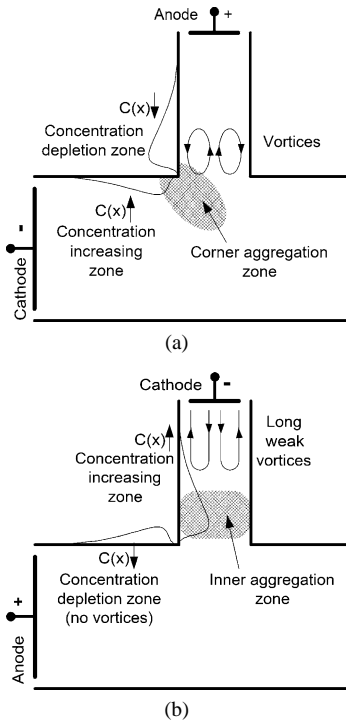


Fig. 3. Vortices in the narrow channel for different electrode configurations and different channel ζ potentials.

With the electrode configuration in Fig. 1, these vortices appear at the junction end. With polarity reversal, the vortices would lie in the remaining part of the channel. These latter vortices would be extremely long and weak. Hence, the electrode configuration in Fig. 1 is most suitable to create relatively short and intense vortex pairs. The circulation direction of these shorter vortices depends on the sign of the ζ potential. With a negative ζ and an electroosmotic flow out of the narrow channel, the tangential velocities of the vortices at the wall are in the original electroosmotic flow direction. These possible scenarios are depicted in Fig. 3.

We will further expound the vortex formation mechanism for the original electrode configuration in Figs. 1 and 3a. The ion concentration is uniform and the potential gradient is constant along the flow direction away from the junction. However, near the junction, there is field leakage out of the inner wall of the narrow channel and field leakage into the inner wall of the wide channel. As a result, the electromigration of ions is smaller in the narrow channel and larger in the wide channel. To maintain constant current flux, these unequal electromigrations must be compensated for by opposite diffusive flux. Hence, concentration gradients are established near the junction but in opposite directions across the junction. The ion concentration increases at the inner wall of the wide channel to reduce the enhanced electromigration flux and decreases on the narrow channel side to enhance the net flux. However, due to its considerable width, concentration accumulation near the inner wall does not affect the average tangential field in the wide channel. Concentration depletion near the inner wall, however, significantly increases

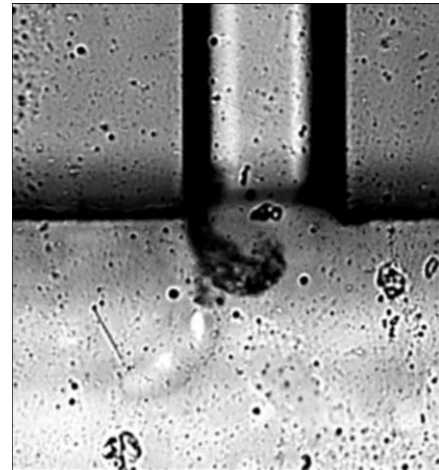


Fig. 4. A symmetric colloidal aggregate at the inside corner for $E_0 = 80 \text{ V/cm}$.

the average tangential field of the narrow channel due to the reduced conductivity. It produces in the narrow channel a higher electroosmotic flow near the junction than away from the junction. Note that this electroosmotic flow is toward the wide channel. To ensure flow balance, a back pressure must build up near the junction in the narrow channel. The mixed pressure-driven and electroosmotic flow leads to corner vortices, as argued in Fig. 2 and shown in Fig. 3a. These corner vortices tend to trap the latex colloids entering from the wide channel at the inner corner and a large aggregate is expected to form at the corner, as we observe in Fig. 4. This scenario is shown in Fig. 3a. Since electroosmotic flow is in a specific direction determined by the field direction and since the two channels are of different widths and different sensitivities to field leakage, reversal of the electrodes polarity leads to a qualitatively different scenario (see Fig. 3b). The ion concentration changes in both channels now reverse, but vortices do not develop in the wide channel, as the average field across the channel is not altered significantly due to the large width. A long and weak recirculation now develops away from the junction in the narrow channel. We observe that large aggregates do not form at the corner for this configuration. Instead, the narrow channel mouth is filled with continuously growing aggregates that eventually block the channel. They are blocked by the long recirculation as shown in Fig. 3b. The scenarios presented above depend not only on the microchannel geometry and electrolyte solution properties, but also on the flow direction determined by the sign on the zeta potential (i.e., material properties) of the channel. Change of sign of the zeta potential would produce an electroosmotic flow toward the narrow channel. The vortices would still exist at the same locations for a specific electrode configuration but would simply change their direction of circulation.

If the penetration length is much smaller than the width of the narrow channel, microvortices the size of the penetration length will still appear [12]. However, because the ion flux through the channel is not affected by these microvor-

tices, the concentration remains uniform across the corner. A macroscopic gradient in the ζ potential and the bulk electroosmotic flow hence cannot appear to produce large vortices that bridge the entire channel. The size of the vortices (whether they span the narrow channel) hence distinguishes these two kinds of vortices. Their locations and symmetries are also different. The larger vortices can only exist within the small channel whereas the microvortices should straddle the cusp of the corner. The circulation directions can also be opposite to each other, as their Smoluchowski velocity gradients can be different at the wall. The larger vortices are more effective for reagent mixing purposes.

These concepts can produce an estimate of the critical electric field for vortex formation if a unidirectional electric field and other simplifications are assumed within the narrow channel. We first set the current density J in (6), which includes both electro-migration and diffusion, to the Ohmic version with a uniform concentration field (14), which is equal to $\sigma(d\varphi_{\text{Ohm}}/dx)$ in the x -direction along the narrow channel. Dividing the resulting equation by C and approximating

$$-\frac{\sigma}{C} \frac{d\varphi_{\text{Ohm}}}{dx} \quad \text{by} \quad -\frac{\sigma}{C_\infty} \frac{d\varphi_{\text{Ohm}}}{dx}$$

(small deviation from Ohmic conditions), the equation becomes an exact differential and can be integrated to yield the relationship between ion concentration depletion and the local field,

$$\frac{\sigma}{C_\infty} d(\varphi - \varphi_{\text{Ohm}}) = -Fz(D_+ - D_-) d \ln C, \quad (22)$$

where the conductivity σ in (14) for the Ohmic condition has been used. Integrating (22) from a location far from the junction, where $\varphi = \varphi_{\text{Ohm}}$ and $C = C_\infty$, to the corner where the potential deviates most from the Ohmic value, we obtain a Boltzmann-like expression with a potential weighted by the difference in the ion diffusivities,

$$\frac{C^*}{C_\infty} = \exp \left[-\frac{Fz^2}{RT} \left(\frac{D_+ + D_-}{D_+ - D_-} \right) (\varphi^* - \varphi_{\text{Ohm}}) \right], \quad (23)$$

where the superscript * denotes corner values. This estimates the concentration depletion at the corner if $\varphi^* - \varphi_{\text{Ohm}}$ is known. The valency z^2 can be set to unity in most cases when the cations are mostly protons and a symmetric electrolyte is assumed. It is also clear that the required potential deviation from the Ohmic value decreases with decreasing diffusivity difference.

For the low ζ potential dielectrics considered here, the local ζ potential scales as $C^{-1/2}$ (see Israelachvili [13], for example). As a result, one could combine criteria (21) and (23) to yield a critical corner potential for vortex formation for the configuration of Fig. 1,

$$\varphi^* - \varphi_{\text{Ohm}} = \frac{RT}{Fz^2} \left(\frac{D_+ - D_-}{D_+ + D_-} \right) \ln 9. \quad (24)$$

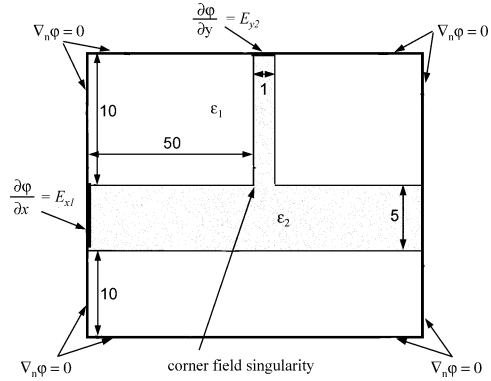


Fig. 5. Computational domain with a normalized coordinate scaled by the width of the narrow channel.

For univalent symmetric electrolytes, $z = 1$, and the corner potential would need to exceed its Ohmic counterpart by

$$\frac{RT}{F} \ln 9 \left(\frac{D_+ - D_-}{D_+ + D_-} \right).$$

For the distilled water used in our experiments, $D_{\text{H}^+}/D_{\text{OH}^-} = 1.8$ (H^+ is about $9.3 \times 10^{-5} \text{ cm}^2/\text{s}$ and OH^- $5.2 \times 10^{-5} \text{ cm}^2/\text{s}$), and the critical excess potential at the corner is $0.6(RT/F)$ or roughly 16 mV. Due to all the assumptions made, this is a rough estimate of the required potential increase due to field leakage. Nevertheless, we expect it to be around 10 mV, which is sufficiently small to be realizable in microfluidic chips.

It remains to determine the corner potential φ^* from the electrostatic problem (1) for a specific microchannel junction geometry. In Fig. 5, we depict our computational domain for our specific geometry in Fig. 1 for a numerical resolution with constant electric fields at the indicated locations. As long as the penetration length is much smaller than the computational domain, the actual electrodes do not need to appear in the domain—the electric fields at the ends of narrow and wide channels are at the Ohmic values in the computational domain. The length scales in the computational domain of Fig. 5 have been normalized by the width of the narrow channel. The boundaries of the computational domain are, however, a distance of 1.5 cm from the anode in the narrow channel and a distance of 1 cm from the cathode in the wide channel. The imposed boundary electric fields in the computation are derived from these lengths. The reported applied electric field E_0 is the total voltage across the electrode divided by the actual lengths of the long and short channel. It has a value in between the two Ohmic fields at the ends of the two channels, which are themselves inversely proportional to the channel widths. The reported potentials from the computation are the actual potential values.

For the electric field calculations, we have solved a Laplace boundary problem using a MATLAB finite-element code. The code produces a sequence of adaptive triangular meshes. The first mesh is an arbitrary triangle array. Subsequent triangular meshes are obtained adaptively during the solution of the problem. New triangular meshes are gener-

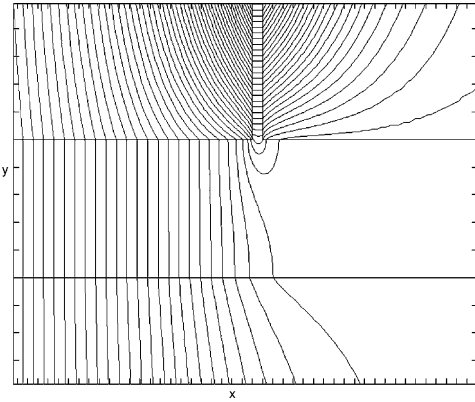


Fig. 6. Computed potential fields for a relative solid permittivity $\varepsilon_r = 3.5$ and an applied field of $E_0 = 50 \text{ V/cm}$.

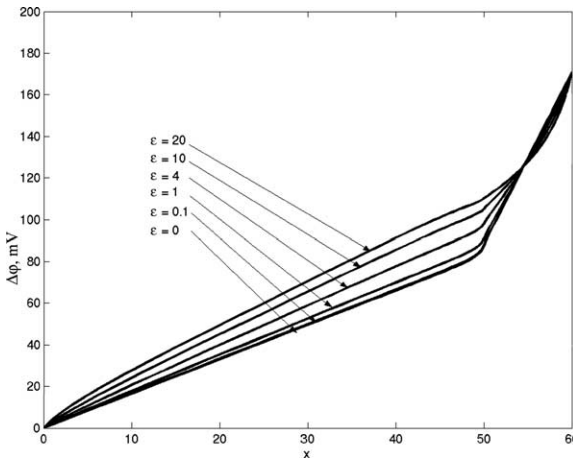


Fig. 7. Potential distribution along the inside wall from the wide channel to the narrow one in a distance scaled by the width of the narrow channel. The distributions correspond to $E_0 = 80 \text{ V/cm}$ and $\varepsilon_r = 0, 10^{-1}, 1, 4, 10$, and 20 .

ated from an error estimate. The iteration continues until the required accuracy is reached, when the relative error does not exceed 10^{-5} . The double layer is neglected in the computation.

A typical computed potential field φ is shown in Fig. 6 in the normalized coordinates of the computational domain of Fig. 5. The potential distribution from the wide channel to the narrow one along the inside wall is shown in Fig. 7 for an applied field $E_0 = 80 \text{ V/cm}$ in the normalized distance scaled by the width of the narrow channel. The dependence on the relative solid permittivity is shown at a constant applied field E_0 . It is clear that an insulated wall would produce an Ohmic field everywhere. This field is constant along each channel but the constant is inversely proportional to the width and is hence different. There is hence a discontinuity in the tangential field at the corner at 50 units of normalized distance from the end of the wide channel. With increasing solid permittivity, however, the discontinuity relaxes into a smooth potential distribution. The electric field near the junction is now higher than the Ohmic value in the wide channel and lower in the narrow channel. This results in a

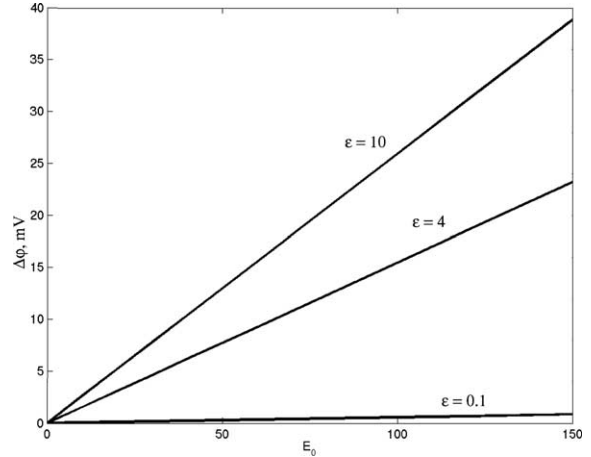


Fig. 8. Excess corner potential (the value by which it exceeds the Ohmic potential for insulated walls) as a function of applied field E_0 for different solid permittivities. The critical applied field of 50 V/cm yields a corner potential $\varphi - \varphi_{\text{Ohm}}$ of $0.6(RT/F) = 16 \text{ mV}$ for a solid permittivity of 4.

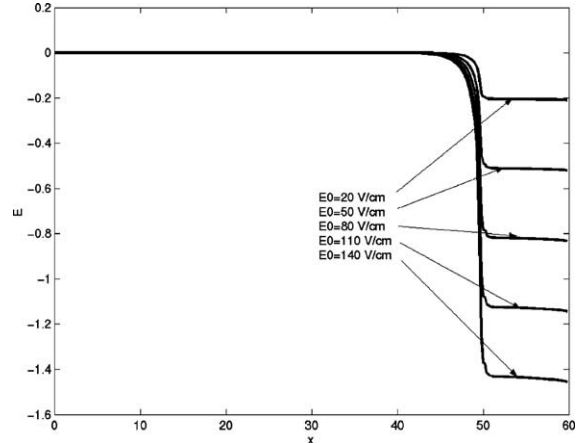


Fig. 9. The normalized inside wall electric field at different E_0 for a solid permittivity of 4.

corner potential higher than the Ohmic value and depletion according to (23). These phenomena are all due to field leakage across the corner. If the polarity of the electrodes were reversed, the field would increase in the narrow channel and decrease in the side channel due to field leakage. The corner potential would then be lower than the Ohmic value, giving rise to an electrolyte buildup according to (23).

In Fig. 8, we depict the excess potential (the amount by which it exceeds the Ohmic value for insulated walls) as a function of the solid permittivity and applied field. In Fig. 9, the electric field along the inside wall for our relative solid permittivity of 4 but with different applied electric fields E_0 is shown. As expected, the amount by which the corner potential exceeds the Ohmic value increases with E_0 , reflecting increasing leakage. At $E_0 = 130 \text{ V/cm}$, this difference exceeds the critical value of $0.6(RT/F) \sim 16 \text{ mV}$ in (24). This is a rough estimate of the critical field for vortices to appear at the junction end of the narrow channel. To further verify that the penetration length exceeds the unit narrow channel

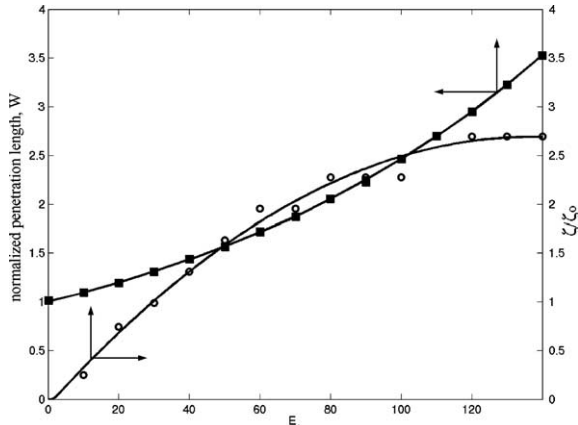


Fig. 10. The normalized corner zeta potential and the corner penetration length ω (defined by the radius of curvature of the potential field) as a function of applied field E_0 .

width, we define the penetration length ω as the width of the electric field distribution in Fig. 9, where the derivative exceeds 0.05. This penetration length is shown as a function of E_0 in Fig. 10. It is clear that by $E_0 = 30$ V/cm, the penetration length has exceeded the width of the narrow channel.

In the same Fig. 10, we depict the corner ζ potential, estimated from the corner potential from (23) and a $C^{-1/2}$ scaling, for a solid relative permittivity of 4 and a liquid permittivity of 81. It is clear that the relative acrylic ζ potential, normalized by the original value, reaches the critical value of 3 in (21) at 130 V/cm. Our estimate of the critical field is expected to be an overestimate. When electrolyte depletion occurs the reduction in conductivity is expected to increase the electric field in the narrow channel by several factors, as the concentration decreases by the same factors. As seen in Fig. 7, a higher field in the narrow channel would increase the potential difference from the Ohmic value. We hence expect the actual critical field to be below 100 V/cm.

4. Experimental verification

We fabricated the junction in Fig. 1 on a modified acrylic sheet. Standard measurements indicate its negative ζ potential is in the range -20 to -25 mV with our distilled water electrolyte. To visualize the streamlines, we inject a colloidal suspension of latex particles into the distilled water. The particles have an average diameter of 500 nm and also have a negative ζ potential. Hence, while the electroosmotic liquid flow is toward the cathode in the wide channel, the electrophoretic motion of the particles is toward the anode in the narrow channel.

After the microchannels are etched into the acrylic sheet, the entire network is filled with distilled water and the surface is then sealed with an adhesive film. Holes are drilled into the film above two reservoirs at the electrode locations and drops of latex colloidal solutions are introduced at these locations. Upon application of additional solution over the

film, the system is left to sit for 24 h to allow the electrical double layers to equilibrate.

Platinum wire electrodes are inserted into the holes at the reservoir. The electric field reported is taken to be the applied potential difference divided by the total channel length between the two electrodes—it is hence between the fields in the narrow and wide channels. The field E_0 is increased incrementally, within the range 0–130 V/cm, and then decreased incrementally to 0. Ascending and descending data are compared to ensure measurement precision and multiple measurements are carried out to ensure reproducibility.

The flowing liquid is invisible but the colloidal particle trajectories are tracked with our microscope. The latter are a superposition of the electroosmotic fluid velocity and the electrophoretic particle velocity, which are opposite in direction. Nevertheless, the particle trajectories can only exhibit vortices if the streamlines also exhibit vortices. Hence, the onset of vortex breakdown should be captured by the particle trajectories.

We observe the colloidal particles to migrate from the wide channel into the narrow channel at low electric fields, as is consistent with a negative latex particle zeta potential. Its absolute value must exceed that of the acrylic wall for the particles to move against the electroosmotic velocity. However, particle trajectories in the osmotic velocity direction are observed at the inside corner at high fields when vortices develop. This is only possible if the local electroosmotic velocity in the opposite direction (from the narrow channel into the wide one) exceeds that of the colloid electrophoretic velocity. The relative magnitudes of the two zeta potentials with opposite signs seem to change with the applied fields.

Particle aggregation is observed at the inside corner beyond 50 V/cm. An image of the unique aggregation pattern is shown in Fig. 4. The aggregate size grows with electric field as shown in the schematics of Fig. 11. By 90 V/cm, it has grown to such a size that the vortices of Figs. 2 and 3 are suppressed by the aggregates. Beyond 110 V/cm, the junction is completely blocked and the colloidal particles are observed to migrate in the opposite direction (away from the narrow channel) even in the wide channel far from the junction. These aggregates are small in dimension and are initially symmetric about the inside corner. They are hence not a result of the large vortices in the narrow channel in Fig. 3 due to electrolyte depletion. They are more likely the result of microvortices at the cusp [12].

Figure 12 depicts actual images of the particle trajectories at $E_0 = 20$ V/cm (a) and 80 V/cm (b). In Fig. 13, the particle trajectories for a range of electric fields are sketched in schematics. At lower fields, the particle trajectories at the junction end of the narrow channel resemble the Ohmic electric field lines and hence the electroosmotic streamlines. However, closed particle trajectories forming large vortices begin to appear beyond 30 V/cm in the narrow channel. They appear in pairs but the vortex at the inside corner is larger and more intense in circulation. The particle velocity around the closed trajectory is not constant. It is much faster

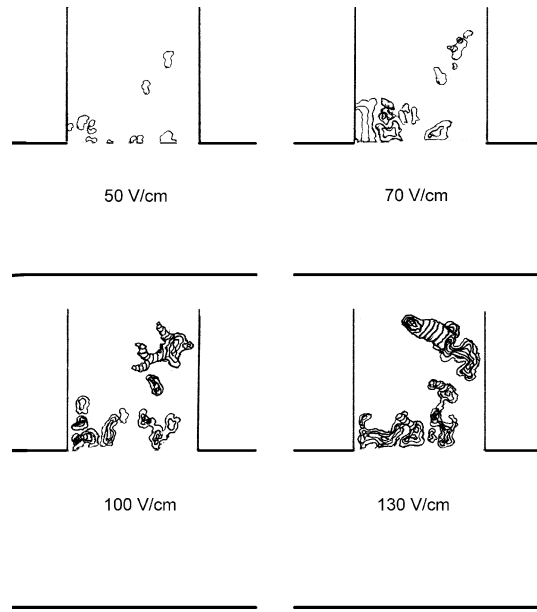


Fig. 11. Schematic depicting the growth of the colloidal aggregate toward the outside corner with increasing E_0 .

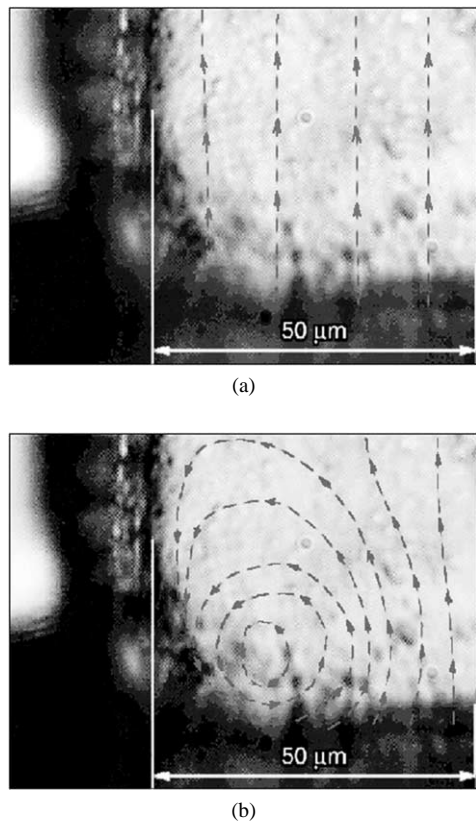


Fig. 12. Colloidal particle images at (a) $E_0 = 20 \text{ V/cm}$ and (b) $E_0 = 80 \text{ V/cm}$ showing symmetric vortices at the higher field.

toward the narrow channel and much slower toward the wide channel near the wall. This suggests that the fluid velocity and the electrophoretic motion are in the same direction away from the wall—evidence of pressure-driven back flow

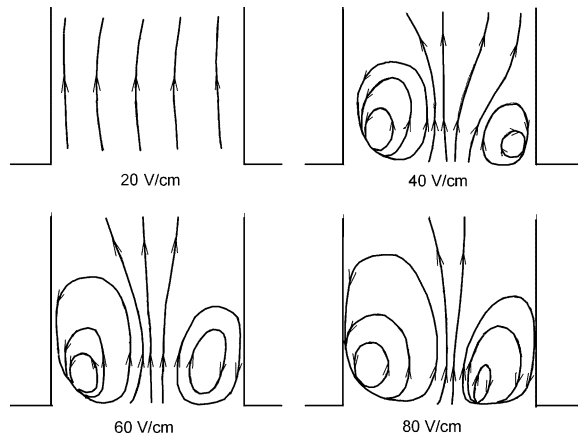


Fig. 13. Schematic for the particle trajectories in the junction end of the narrow channel.

in the middle of the channel, as shown in Fig. 2. Beyond 90 V/cm , the circulations vanish as the corner colloidal aggregates grow to significant dimensions.

If we reverse the polarity of the electrodes, the vortices are never observed. This is again consistent with our arguments summarized in Fig. 3. The long slender vortices away from the junction are theoretically possible but are extremely weak and hence suppressed by the electrophoretic velocity.

The experimental critical field for the large vortices is hence about $E_0 = 30 \text{ V/cm}$. The corner aggregates are, however, observed beyond $E_0 = 50 \text{ V/cm}$. We had expected these small corner vortices to appear much earlier when the penetration length ω is less than the width of the narrow channel. However, the microvortices are too small to be observed and their onset does not necessarily correspond to the beginning of colloid aggregation. The corner colloidal aggregates are also affected not only by the microvortices but also by the large vortices. Moreover, the electrophoretic motion of the colloids and even their polarization may affect their aggregation. One hence cannot attach too much significance to the critical field of $E_0 = 50 \text{ V/cm}$ for colloid aggregation.

5. Summary and discussion

There is also a possibility that the observed vortices are due to natural thermal convection. Joule heat generation occurs in our system as it does in all electrochemical/electrotransport systems, but the heat generation is uniformly distributed all over the microfluidic system. Moreover, natural thermal convection has certain specific features—it is associated with density variation and it has a large component of motion along the direction of gravity (normal to the chip). Microscopy observations have not detected any local changes in the optical density of the solution at the intersection. All tracer particles trajectories are also observed to follow the electric field streamlines tangent

to the plane of the chip, without any normal component indicative of convection motion.

The breakdown of the coincidence between electric field lines and Ohmic electroosmotic streamlines in electrically insulated channels also means the irrotational character of the flow is violated. We exploit this observation by producing vortices near corners. Leakage across the solid is most severe at corners and the departure from Ohmic streamlines is most drastic. We observe colloidal aggregation at the inside corner of a junction that is speculated to be due to a microvortex formation mechanism with uniform concentration. Larger vortices at the junction end of the narrower channel connected to the corner are also observed. These are shown to be due to electrolyte depletion and ζ potential elevation effects of current leakage when the penetration length is longer than the channel width. We note from Fig. 7 that this leakage is most pronounced when the two channels have widely different widths, so that the two far-field electric fields have very different values. An onset criterion for the large vortices is established and favorably compared to experimental data. These vortices and even the through flow will eventually be disrupted by the corner colloid aggregates. Mixing elements that utilize these vortices must hence operate within this field window. The intensity of the vortices should increase when the turn angle becomes more acute. We leave this optimization problem for a later publication.

Acknowledgments

This work is supported by an NSF XYZ-on-a-Chip grant. We are grateful to Justin Burt for making some of the measurements.

References

- [1] H.A. Stone, S. Kim, *AIChE J.* 6 (2001) 1250.
- [2] M. Trau, B.J. Battersby, *Adv. Mater.* 13 (2001) 975.
- [3] A. Dodge, K. Fluri, E. Verpoote, N.F. de Rooij, *Anal. Chem.* 73 (2001) 3400.
- [4] P.V. Takhistov, A. Indeikina, H.-C. Chang, *Phys. Fluids* 14 (2002) 1.
- [5] R.F. Probstein, *Physicochemical Hydrodynamics—An Introduction*, Butterworths, Boston, 1989.
- [6] H.-C. Chang, in: M. Gad-el-Hak (Ed.), *CRC MEM Handbook*, CRC Press, Boca Raton, FL, 2001, Chap. 11.
- [7] D. Dutta, D.T. Leighton, *Anal. Chem.* 73 (2001) 3400.
- [8] A.E. Herr, J.I. Molho, J.G. Santiago, M.G. Mungal, T.W. Kenny, M.G. Garguilo, *Anal. Chem.* 72 (2000) 1053.
- [9] J.L. Anderson, W.K. Idol, *Chem. Eng. Commun.* 38 (1985) 93.
- [10] Y. Ben, E.A. Demekhin, P.V. Takhistov, H.-C. Chang, *J. Chin. Inst. Chem. Eng.* 33 (2002) 203.
- [11] J.T.G. Overbeek, in: H.R. Kruyt (Ed.), in: *Colloid Science*, Vol. 1, Elsevier, Amsterdam, 1952.
- [12] S. Thamida, H.-C. Chang, *Phys. Fluids* 14 (2002) 4315.
- [13] J.N. Israelachvili, *Intermolecular and Surface Forces*, Academic Press, London, 1991.
- [14] E.B. Cummings, S.K. Griffiths, R.H. Nilson, P.H. Paul, *Anal. Chem.* 72 (2000) 2526.